Turbulent fronts in resonantly forced oscillatory systems

Christopher Hemming and Raymond Kapral

Chemical Physics Theory Group, Department of Chemistry, University of Toronto, Toronto, ON M5S 3H6, Canada

Received 10th April 2001
First published as an Advance Article on the web 7th November 2001

Phase fronts in the forced complex Ginzburg–Landau equation, a model of a resonantly forced oscillatory reaction–diffusion system, are studied in the 3 : 1 resonance regime. The focus is on the turbulent (Benjamin–Feir-unstable) regime of the corresponding unforced system; in the forced system, phase fronts between spatially uniform phase-locked states exhibit complex dynamics. In one dimension, for strong forcing, phase fronts move with constant velocity. As the forcing intensity is lowered there is a bifurcation to oscillatory motion, followed by a bifurcation to a regime in which fronts multiply *via* the nucleation of domains of the third homogeneous phase in the front. In two dimensional systems, rough fronts with turbulent, complex internal structure may arise. For a critical value of the forcing intensity there is a nonequilibrium phase transition in which the turbulent interface grows to occupy the entire system. The phenomena we explore can be probed by experiments on periodically forced light sensitive reaction–diffusion systems.

1 Introduction

Resonant forcing of oscillatory reaction–diffusion systems can lead to a variety of chemical patterns not seen in unforced systems. In a well-stirred system, an external periodic perturbation, sufficiently close to the resonant frequency, causes phase-locking of the oscillatory kinetics. At the $n : m$ resonance stable oscillations may occur only with one of n different phases. These n stable phase states are equivalent under phase shifts of $2\pi/n$.

In a reaction–diffusion system, a spatially-distributed field of these local n-stable oscillators is coupled by diffusion. The system tends to form spatially uniform domains inside which the local oscillations are synchronized to one of the phase-locked states. The boundaries between domains, where the phase of the oscillations shifts, are domain walls or "phase fronts". Such phase fronts have been observed in experimental studies of the ruthenium-catalyzed Belousov–Zhabotinsky reaction in a continously-fed open reactor, illuminated with a periodic light source.[1–4]

In many cases the dynamics of patterns in the system can be understood in terms of the dynamics of the phase fronts. For example, a transition between labyrinthine and non-labyrinthine stationary two-phase patterns in experiments in 2 : 1 forced systems was attributed to a lateral instability in the phase front.[2] Travelling loop structures in 2 : 1 experiments were ascribed to the presence of a nonequilibrium Ising–Bloch front bifurcation.[5] Earlier theoretical work had predicted that such a bifurcation could exist in 2 : 1 phase fronts.[6]

In this paper, we describe phase fronts in the resonantly forced complex Ginzburg–Landau

(FCGL) system

$$\frac{\partial A(\boldsymbol{r}, t)}{\partial t} = (\mu + \mathrm{i}\nu)A - (1 + \mathrm{i}\beta)|A|^2 A + \gamma \bar{A}^{n-1} + (1 + \mathrm{i}\alpha)\nabla^2 A. \quad (1)$$

This equation describes the envelope of oscillations of a forced system at the $n : m$ resonance (n, m are coprime integers, $n \leqslant 4$) near the Hopf bifurcation.[7,8] The parameter γ is the amplitude of the forcing. The reagent concentrations $\boldsymbol{c}(\boldsymbol{r}, t)$ in the original reaction–diffusion system which the complex Ginzburg–Landau equation models are related to the complex amplitude $A(\boldsymbol{r}, t)$ according to

$$\boldsymbol{c}(\boldsymbol{r}, t) - \boldsymbol{c}_0 \approx A\boldsymbol{u}\mathrm{e}^{\mathrm{i}\omega_\mathrm{f} t/n} + \bar{A}\bar{\boldsymbol{u}}\mathrm{e}^{-\mathrm{i}\omega_\mathrm{f} t/n}, \quad (2)$$

where $\boldsymbol{u}$ and $\bar{\boldsymbol{u}}$ are the critical eigenvectors involved in the Hopf bifurcation and $\omega_\mathrm{f} \approx n\omega_0/m$ is the forcing frequency. As well as being the normal form of the bifurcation, eqn. (1) is widely used as a generic model of resonantly forced oscillatory reaction–diffusion systems. In the remainder of this paper we focus on the $n = 3$ case corresponding to the 3 : 1 resonance.

The ordinary differential equation (ODE) describing the local dynamics of the medium in the absence of diffusion, $\mathrm{d}A/\mathrm{d}t = (\mu + \mathrm{i}\nu)A - (1 + \mathrm{i}\beta)|A|^2 A + \gamma \bar{A}^{n-1}$, has only the trivial fixed point $A = 0$ for $\gamma = 0$. As γ increases, there is a bifurcation where n pairs of fixed points appear. From eqn. (2) we see that these fixed point solutions correspond to phase-locked oscillatory solutions in the original forced reacting system that is modelled by the reduced FCGL dynamics. The phase shift symmetry under $t \rightarrow t + 2\pi/\omega_\mathrm{f}$ in the reacting system system appears in the FCGL equation as the phase shift symmetry $A \rightarrow A\mathrm{e}^{2\mathrm{i}\pi/n}$; hence, we consider the FCGL equation to describe the dynamics of the original system viewed stroboscopically in Poincaré planes taken at intervals $\Delta t = 2n\pi/\omega_\mathrm{f}$. The FCGL equation exhibits spatially uniform phase-locked domains and phase fronts which correspond to those observed in resonantly-forced reaction–diffusion systems.

The unforced CGL equation (eqn. (1) with $\gamma = 0$), exhibits phase turbulence in the Benjamin–Feir-unstable regime, which is the region of parameter space in which $1 + \alpha\beta < 0$. If forcing is added to the CGL equation in the Benjamin–Feir-unstable regime (*i.e.* if γ is taken to be nonzero) the synchronizing effect of the forcing opposes the desynchronizing effect of the turbulent CGL dynamics. Coullet and Emilsson investigated eqn. (1) in this regime.[9–11] In the one-dimensional case, when the forcing intensity is high, one observes phase fronts which either may be stationary or may translate monotonically with a constant velocity v and have a front profile $A(x, t) = A(x - vt)$. This behavior is identical to the Benjamin–Feir-stable case.[12] For $n = 2$, as γ is lowered, one observes a Hopf bifurcation in which an oscillatory motion is superposed on the translating (or stationary) front motion. As γ is decreased further a series of period-doubling bifurcations occurs. Eventually chaotic motion of the front ensues. At still lower γ, a regime in which a turbulent region is nucleated at the front is observed, and ultimately the turbulent region expands to fill the system. The dynamics of phase fronts in the $n = 2$, $d = 1$ system was also investigated by Mizuguchi and Sasa[13] and Battogtokh and Browne[14]. Phase fronts in two dimensions exhibit spontaneous roughening of the front profile.[9]

Phase front roughening in two dimensions has been observed in a coupled map lattice (CML) system which may be regarded as a model for a periodically forced oscillatory system.[15–18] If the uncoupled map is chosen such that it possesses a superstable period-3 cyclic solution $1 \rightarrow 2 \rightarrow 3 \rightarrow 1$, there are three cyclic solutions differing in phase by one discrete time step. In this sense the map is a model for a 3 : 1 resonantly forced oscillator. In two dimensions, the fronts exhibit a variety of other dynamical phenomena, including a nonequilibrium phase transition to a regime of strong turbulence. Before the transition, interfaces between spatially uniform regions are rough. As a control parameter is varied, the intrinsic width of the interface increases and complex, irregular structure develops. As the transition is approached the width of the complex, disordered interfacial zone increases. The intrinsic interface width diverges at the transition; beyond the transition the spatially uniform phases are unstable relative to the turbulent phase; hence, an initially present interface will grow to fill the entire system with the turbulent phase. In this paper we show that qualitatively similar phenomena are found in the 3 : 1 FCGL system.

Section 2 is devoted to a study of the one-dimensional, $n = 3$, FCGL equation. In Section 3 we consider phase fronts in two-dimensional systems and in Section 4 we discuss the strong turbu-

lence regime found beyond the nonequilibrium phase transition. The conclusions of the paper are given in Section 5.

2 One-dimensional fronts

We consider first the simplest case: eqn. (1) with μ, ν, α and β such that the unforced ($\gamma = 0$) equation is in the Benjamin–Feir-stable regime. For $\gamma > [2((1 + \beta^2)(\mu^2 + \nu^2))^{1/2} - 2(\mu + \beta\nu)]^{1/2}$, the corresponding ODE $\mathrm{d}A/\mathrm{d}t = (\mu + \mathrm{i}\nu)A - (1 + \mathrm{i}\beta)|A|^2A + \gamma\bar{A}^2$ possesses 3 stable fixed points A_0^i, $i = 1, 2, 3$ (and 3 corresponding unstable ones, as well as the unstable $A = 0$ fixed point) which are also solutions of the spatially distributed system. These solutions are linearly stable to spatially homogeneous perturbations, and in the Benjamin–Feir-stable regime are stable to spatially inhomogeneous perturbations. In one dimension, the next simplest solution is a front joining two of these spatially uniform states. These phase fronts travel at a constant velocity v with constant shape, $A(x, t) = A(x - vt)$.

When the unforced system is Benjamin–Feir-unstable, such uniformly translating front solutions are stable for large values of γ. Fig. 1 shows such a front solution for the parameter values $\mu = 1$, $\nu = 1.55$, $\alpha = -1.3$, $\beta = 1.5$ and $\gamma = 0.63$. Throughout this paper we fix μ, ν, α and β at these values; γ is taken to be the control parameter.†

As γ is lowered, a bifurcation to oscillatory front motion occurs at γ_c. In general, these oscillating fronts have a non-zero average velocity. In the $n = 2$ case, a Hopf bifurcation to oscillatory motion was found.[9,10,13] However, in the $n = 3$ system the bifurcation is not a Hopf bifurcation: the period T of the oscillations diverges as $T \sim |\gamma_c - \gamma|^{-1/2}$ as $\gamma \to \gamma_c^-$ (Fig. 2 (left)). At the bifurcation, the average front velocity, scales as $v - v(\gamma_c) \sim a_\pm |\gamma_c - \gamma|^{1/2}$ (Fig. 2 (right)), where $a_\pm$ depends on the sign of $\gamma_c - \gamma$.

For yet lower γ a bifurcation to a regime of weak turbulence occurs (see Fig. 3). The mechanism for the appearance of weak turbulence involves the nucleation of a finite-sized domain of the third phase at the front. For example letting [12] denote a front separating phases 1 and 2, nucleation of phase 3 at the front leads to a [13···32] front pair, which travels in the opposite direction. These newly-formed fronts subsequently undergo similar nucleation events; in addition fronts may collide and annihilate. Fig. 3 illustrates a number of such front-splitting, reversal, and annihilation events. One can see that the number of fronts increases and that the size of the region in which fronts are found increases. In this weakly turbulent region the front splitting and reversal events exhibit complex dynamics. A front-splitting regime of this kind has not been reported for the

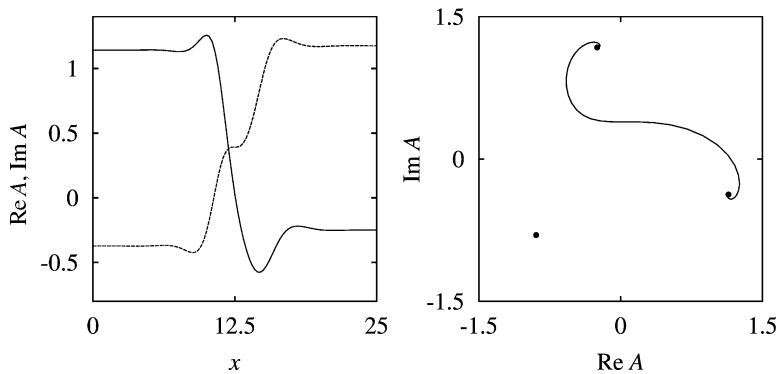

Fig. 1 A travelling front solution in the one-dimensional $n = 3$ FCGL equation for $\gamma = 0.63$. Other parameters are given in the text. Left: Re A (solid line) and Im A (dashed line) against x. Right: The front plotted as a trajectory in the A-plane (solid line); the three filled circles are the three stable spatially uniform states.

† Numerical integration of the FCGL equation was performed using explicit forward differencing with a time step size of $\Delta t = 0.01$. The lattice spacing was $\Delta x = 0.25$ in one dimension. In two dimensions, $\Delta x = 0.25$ or 0.5 and a second-order discrete Laplacian was used. Time intervals and lengths are reported in the absolute time and space units in which eqn. (1) is written.

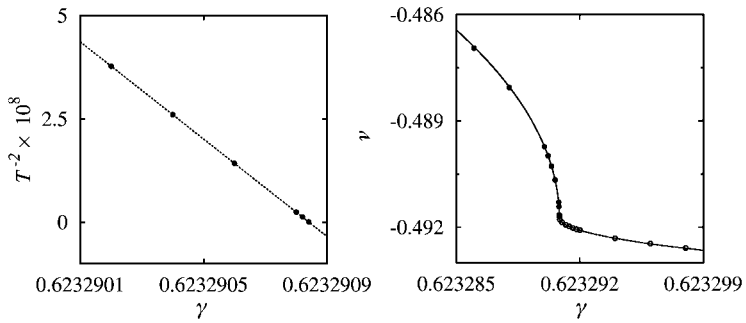

Fig. 2 Left: Plot of T^{-2} against γ, where T is the period of oscillations in the one-dimensional FCGL equation. The filled circles are simulation values, the dotted line is $T^{-2} = 0.058\,881\,76(\gamma_c - \gamma)$, where $\gamma_c = 0.623\,290\,841\,4$. Right: Front velocity v against γ. Circles, simulation values; hollow circles, non-oscillatory regime and filled circles, average velocity in the oscillatory regime. The solid line is the curve $v = v_c + 2.196(\gamma_c - \gamma)^{1/2}$; the dashed line is the curve $v = v_c - 0.3192(\gamma - \gamma_c)^{1/2}$, where $v_c = -0.491\,742$.

$n = 2$ case. The repeated formation of new fronts and spatially homogenous domains observed here bears some resemblance to a mechanism giving rise to spatiotemporal chaos that has been described in a reaction–diffusion system with one stable homogenous state.[19]

Continuing to decrease γ, we encounter windows of regular dynamics within the domain of weakly turbulent dynamics. An interesting localized structure observed was an oscillating hole with zero average velocity within a single phase-locked domain (Fig. 4). This was found at a γ value for which phase fronts are unstable. The character of the spatiotemporal dynamics for

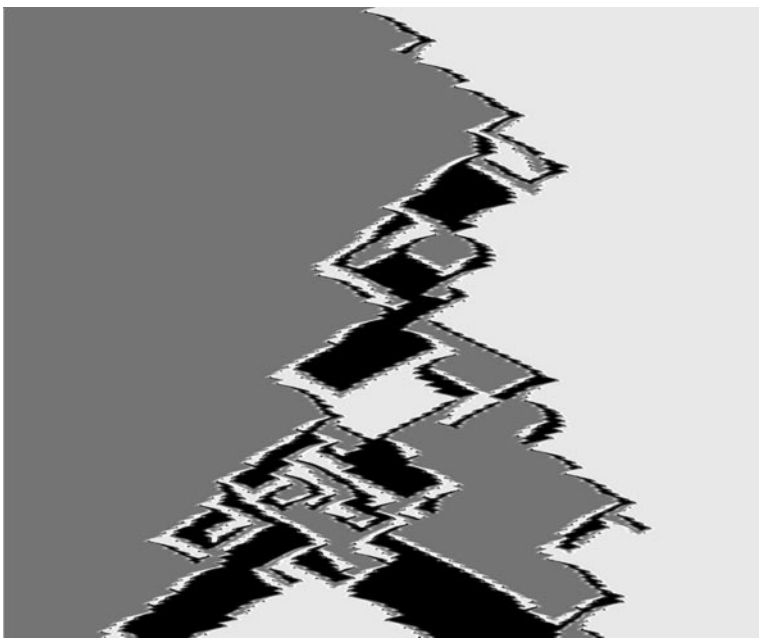

Fig. 3 Space–time plot of the phase ϕ of the complex amplitude $A(x, t) = Re^{i\phi}$ in the one-dimensional FCGL equation for $\gamma = 0.602\,105\,62$. Time is on the ordinate and increases downward. The time interval shown is 2500 time units. The system size is 1250 space units, the plot shows a portion with length 750 space units. The initial conditions were $A(x, 0) = \theta(-x)A_0^L + \theta(x)A_0^R$, where $\theta(x)$ is the Heaviside function and A_0^L and A_0^R, (L, $R \in \{1, 2, 3\}$, $L \neq R$) are the fixed points of the ODE represented by the medium and light grey shades, respectively. The third fixed point is represented by the dark grey shade.

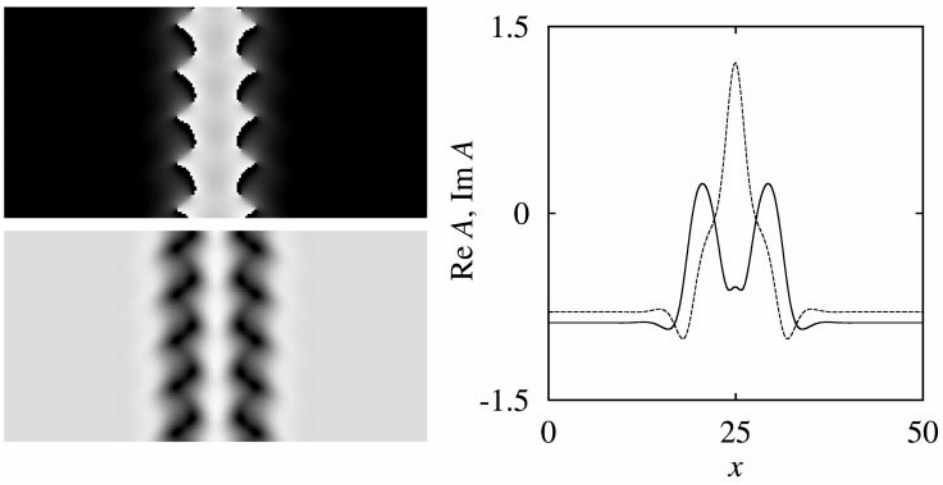

Fig. 4 A zero-velocity hole solution for $\gamma = 0.573$. On the left are space–time plots of the phase (upper panel) and amplitude (lower panel) of A. The plots show an interval of 20 time units. The system size is 1250 space units, the plots show a portion with length 50 units. Right: Graph of Re A (solid line) and Im A (dashed line) against position, recorded at the time at which the space–time plots begin.

$\gamma \approx 0.2$ takes the form of strong turbulence where both the phase and amplitude vary irregularly on short distance and time scales. An example of turbulence of this type is shown in Fig. 5. One can see in this figure that the homogeneous regions within the turbulent phase are rare and short-lived.

Having given this brief overview of the phenomenology of fronts in the one-dimensional system; we consider two-dimensional fronts where new phenomena arise.

3 Two-dimensional fronts

In two spatial dimensions front structure and evolution exhibit a number of distinctive characteristics. For sufficiently high γ planar two-dimensional fronts exist which are similar to those seen in one-dimensional systems. For lower γ, the front profile roughens but the intrinsic width of the front is small and comparable to that of the planar front. The front position oscillates locally but

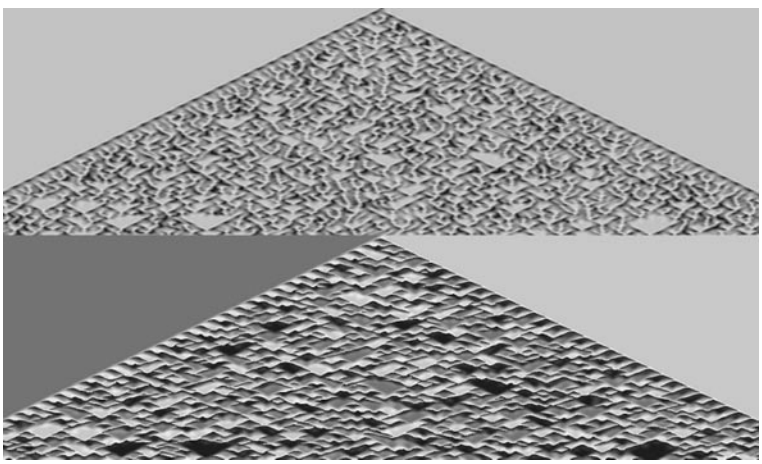

Fig. 5 Space–time plot of the amplitude (upper panel) and phase (lower panel) of the dynamics in the strong turbulence regime for $\gamma = 0.2$. The system size is 1250 space units, the plots show a portion 500 units in length. The time interval is 300 units. The initial conditions were of the form described in the Fig. 3 caption.

these oscillations lose phase-synchronization along the front. Fig. 6 shows typical examples of fronts of this kind for $\gamma = 0.59$.

Decreasing γ further, the average intrinsic width of the fronts increases and complex internal structure develops. In this regime we may regard the front as a turbulent phase separating the two spatially homogenous phases. Fig. 7 shows fronts of this type for $\gamma = 0.46$.

The average width of the interface increases, eventually diverging as $\gamma \to \gamma^*$. For our parameter values $\gamma^* \simeq 0.457$. If $\gamma < \gamma^*$ the turbulent interfacial phase is no longer confined but grows without bound, eventually filling the entire system, regardless of system size. We may regard this "front explosion" as the loss of stability of the homogeneous phases relative to the turbulent phase.

We have statistically characterized the front dynamics for the two confined front regimes mentioned above, using $\gamma = 0.58$ and $\gamma = 0.49$ as representative values of the two cases. Periodic boundary conditions were used in the direction parallel to the front motion and no-flux boundary conditions were imposed on the edges perpendicular to the front motion. The simulations were performed in a frame moving with the front. The initial conditions consisted of domains of the

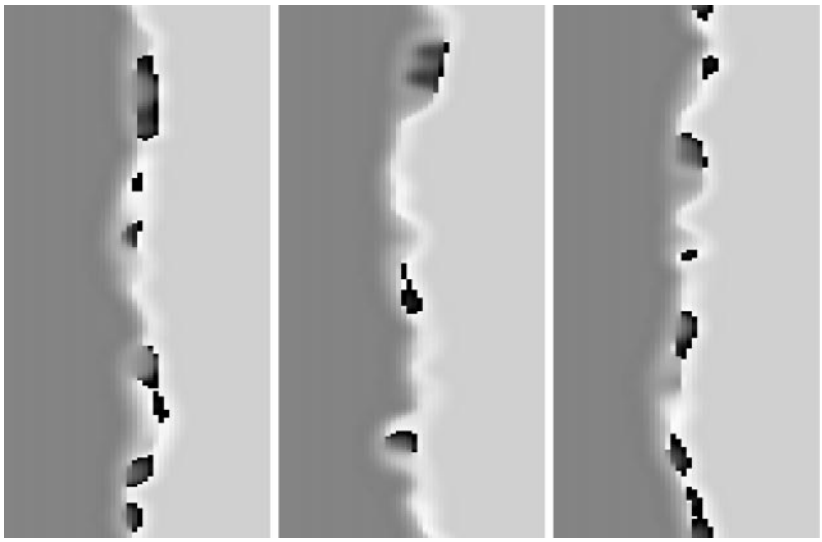

Fig. 6 Typical fronts in the "thin front" regime taken from a single realization of the dynamics at three well separated times. Here $\gamma = 0.59$. The grey-scale indicates the phase ϕ of the complex amplitude $A = Re^{i\phi}$, with $\phi = -\pi$ corresponding to the darkest shade and $\phi = +\pi$ corresponding to the lightest shade. Points around which all shades of grey appear are phase defects. The system size is 200 × 200 space units, a portion with dimensions 100 × 200 is shown.

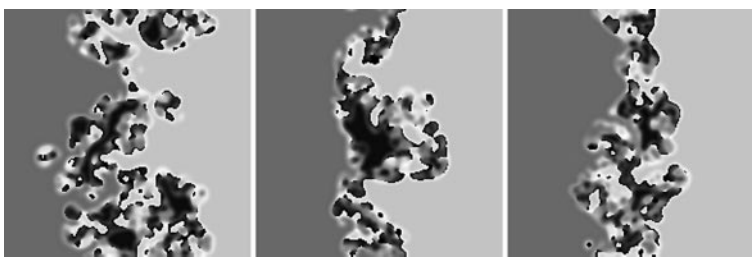

Fig. 7 The turbulent front in a system with $\gamma = 0.46$ at three different times. Grey-scale coding is the same as in Fig. 6. The system size is 800 × 200 space units, a portion with dimensions 200 × 200 is shown.

spatially uniform stable states separated by a randomly seeded planar strip. More precisely,

$$A(x, y, 0) = \begin{cases} A_0^L, & -\infty < x < -W/2 \\ R_0 \, e^{i\phi(x, y)}, & -W/2 \leqslant x \leqslant W/2 \\ A_0^R, & W/2 < x < +\infty \end{cases} \tag{3}$$

where W is the width of the randomly seeded strip, $\phi(x, y)$ is a random variable uniformly distributed on $[-\pi, +\pi)$, A_0^L and A_0^L ($L, R \in \{1, 2, 3\}$) are fixed points of the ODE and $R_0 = |A_0^L| = |A_0^R|$.

We define the position of the right profile $h_R(y, t)$ to be the greatest value of x for which $|A(x, y, t) - A_0^R| \geqslant \varepsilon$. An analogous criterion is used to define the left profile: $h_L(y, t)$ is the smallest value for which $|A(x, y, t) - A_0^L| \geqslant \varepsilon$. The value $\varepsilon = 0.02$ was chosen; comparison of the front profiles determined by this method with the images of the phase and amplitude fields confirmed that this value for ε defined the boundaries of the interfacial zone well.

We also define the mean positions of the left and right profiles, $\bar{h}_{L/R}(t) = L^{-1} \int_0^L dy h_{L/R}(y, t)$, the deviations from the mean, $\delta h_{L/R}(y, t) = h_{L/R}(y, t) - \bar{h}_{L/R}(t)$, and the widths of the left and right profiles,

$$w_{L/R}(t) = \left\{ \frac{1}{L} \int_0^L dy \delta h_{L/R}^2(y, t) \right\}^{1/2}. \tag{4}$$

Diffusively rough interfaces typically obey the following scaling relations:[20] at small t the ensemble average width $\langle w(t) \rangle \sim t^{\hat{\beta}}$, until it saturates at $w_{sat} \sim L^{\hat{\alpha}}$. One may rescale the $\langle w(t) \rangle$ *vs.* t curve by these scaling exponents to obtain $\langle w(t) \rangle / L^{\hat{\alpha}}$ *vs.* $t/L^{\hat{\alpha}/\hat{\beta}}$ which is independent of the system size. Fronts described by the Edwards–Wilkinson (EW) equation[21] have $\hat{\alpha} = 1/2$ and $\hat{\beta} = 1/4$ while Kardar–Parisi–Zhang (KPZ) fronts[22] have $\hat{\alpha} = 1/2$ and $\hat{\beta} = 1/3$.

For $\gamma = 0.58$ ("thin front" case), using both EW and KPZ exponents, neither the left nor the right interfacial profiles yielded data collapse. However, rescaling by the exponents $\hat{\alpha} = 1/2$ and $\hat{\beta} = \hat{\alpha}/3.0 \simeq 0.17$ leads to a reasonable collapse of the $\langle w(t) \rangle$ data (see Fig. 8 (left)), except for the smallest system size, $L = 200$. The oscillations which are clearly visible at early times in the $L = 200$ curve are also present in the data for larger system sizes but are collapsed by the rescaling to a small time interval near the origin and are not visible in the figure. The fact that KPZ exponent scaling fails to provide a data collapse may possibly be ascribed to the correlated nature of the turbulent dynamics driving the front roughening process in the FCGL system. The oscillations present at early times are an indication that the spectrum of the deterministic noise in this system is unlikely to be white.

The above results on the width scaling structure are not generally valid for all fronts observed in this system and the scaling exponents are found to be a function of γ. For example, for $\gamma = 0.49$,

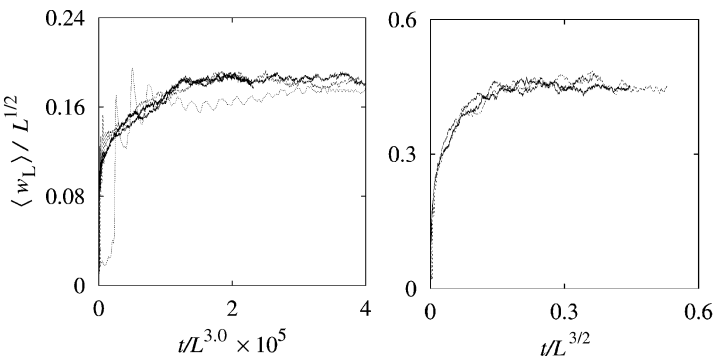

Fig. 8 Left: The scaled left interfacial profile width *vs.* time, $\langle w_L(t) \rangle / L^{1/2}$ *vs.* $t/L^{3.0}$, for system sizes $L = 600$ (solid line), $L = 500$ (long-dashed line), $L = 400$ (short-dashed line) and $L = 200$ (dotted line) for $\gamma = 0.58$. Right: Scaled plot of the average width of the left profile, $\langle w_L(t) \rangle / L^{1/2}$ *vs.* $t/L^{3/2}$ for system sizes $L = 500$ (solid curve), 400 (dashed curve) and 200 (dotted curve) for $\gamma = 0.49$. Each curve is an average over 100 realizations from initial conditions eqn. (3).

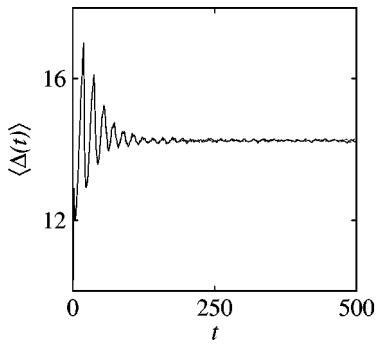

Fig. 9 $\langle\Delta(t)\rangle$ *vs.* t for $L = 400$ (solid line) and $L = 600$ (dashed line) for $\gamma = 0.58$. The average is taken over 100 realizations from initial conditions eqn. (3).

KPZ scaling is found to produce good data collapse (see Fig. 8 (right)). The interface for this parameter value is thick and the internal turbulent structure is more fully developed. As a result the deterministic chaos likely has shorter spatial and temporal correlations making a KPZ approximation to the interfacial dynamics reasonable.

In addition to the average interfacial profile width discussed above we may examine the structure of the intrinsic width of the front $\Delta(y, t)$ which is defined by $\Delta(y, t) = h_R(y, t) - h_L(y, t)$. A plot of $\langle\Delta(t)\rangle$ against t is shown in Fig. 9 for $\gamma = 0.58$. Here $\langle\cdot\rangle$ is an average over the front length and realizations. One observes oscillatory decay to a constant asymptotic value. Note that the curves obtained are essentially indistinguishable for the two different system sizes considered in the figure. The spatial and temporal autocorrelation functions of the intrinsic width are defined by

$$C_\Delta(x) = \langle\delta\Delta(y, t')\delta\Delta(y + y', t')\rangle/\langle\delta\Delta^2\rangle, \tag{5}$$

$$C_\Delta(t) = \langle\delta\Delta(y', t)\delta\Delta(y', t + t')\rangle/\langle\delta\Delta^2\rangle, \tag{6}$$

where the $\langle\cdot\rangle$ represents an average over y' and t' after the front has reached its statistically stationary regime and $\delta\Delta = \Delta - \langle\Delta\rangle$. The temporal and spatial autocorrelation functions are plotted in Fig. 10. From this figure we see that both temporal and spatial autocorrelations decay rapidly and both the correlation time and correlation length increase with decreasing γ. From an examination of instantaneous pictures of the front in Fig. 7 one can see the formation of large fluctuations in the intrinsic interfacial width which extend over long distances. The sizes of these extended turbulent domains increase as γ decreases and this is signalled in the increased correlation length. Similarly, the timescale on which these fluctuations decay increases for lower γ values.

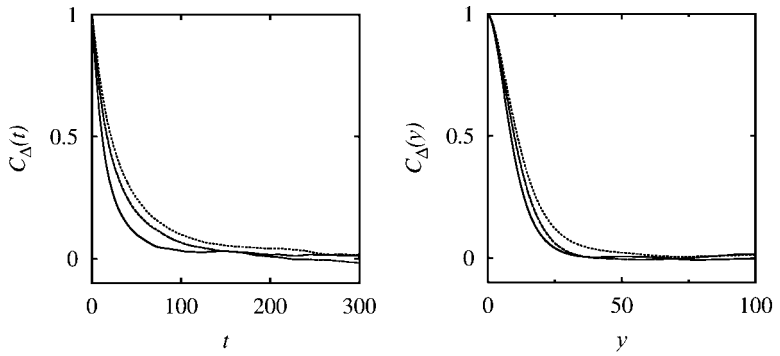

Fig. 10 (left) Temporal autocorrelation function $C_\Delta(t)$ and (right) spatial autocorrelation function $C_\Delta(y)$ for several different γ values: $\gamma = 0.49$ (solid line), $\gamma = 0.48$ (dashed line) and $\gamma = 0.475$ (dotted line). These were measured in simulations in systems of size $L = 200$.

4 The strong turbulence regime in two dimensions

Below $\gamma^* \simeq 0.457$, starting from a planar front separating two stable homogeneous phases, the width Δ increases without bound; thus, the turbulent phase eventually fills the entire system. The time evolution of the front for $\gamma = 0.45$ is presented in Fig. 11 and shows the unbounded growth of the turbulent phase for this γ value. For two-dimensional systems we call this the "strong turbulence" regime. The largest Lyapunov exponent λ in a system containing only the turbulent phase was measured[23] for $\gamma = 0.45$ and found to be $\lambda \simeq 0.31$, signalling the presence of deterministic chaos in this model. Consistent with this, spatial

$$C_A(r) = \langle \bar{A}(\boldsymbol{r} + \boldsymbol{r}')A(\boldsymbol{r}')\rangle / \langle |A|^2 \rangle, \tag{7}$$

and temporal

$$C_A(t) = \langle \bar{A}(t + t')A(t')\rangle / \langle |A|^2 \rangle \tag{8}$$

correlations decay rapidly within the turbulent phase (see Fig. 12).

We have shown in Fig. 11 that the turbulent phase invades the stable homogeneous phases. In this regime there is only one interfacial profile to consider since the turbulent phase is not confined and it is no longer necessary to distinguish left and right interfacial profiles. If the turbulent phase is on the left and the homogeneous phase is on the right, the profile $h(y, t)$ is defined identically to the right profile $h_R(y, t)$ above, *i.e.*, as the greatest x such that $|A(x, y, t) - A_0| > \varepsilon$. It is interesting to investigate the scaling properties of the width of this interfacial profile. The scaling studies were performed starting from initial conditions of the form

$$A(x, y, 0) = \begin{cases} \tilde{A}(x, y), & x \leqslant 0 \\ A_0, & x > 0. \end{cases} \tag{9}$$

where A_0 is one of the stable spatially uniform states, and $\tilde{A}(x, y)$ is a turbulent state prepared by allowing initial conditions of the form

$$A(x, y) = R_0 \, e^{i\phi(x, y)} \tag{10}$$

to evolve under the FCGL dynamics for $t = 200$ time units. In eqn. (10), $R_0 = |A_0|$, and $\phi(x, y)$ is a random variable uniformly distributed on $[-\pi, \pi)$.

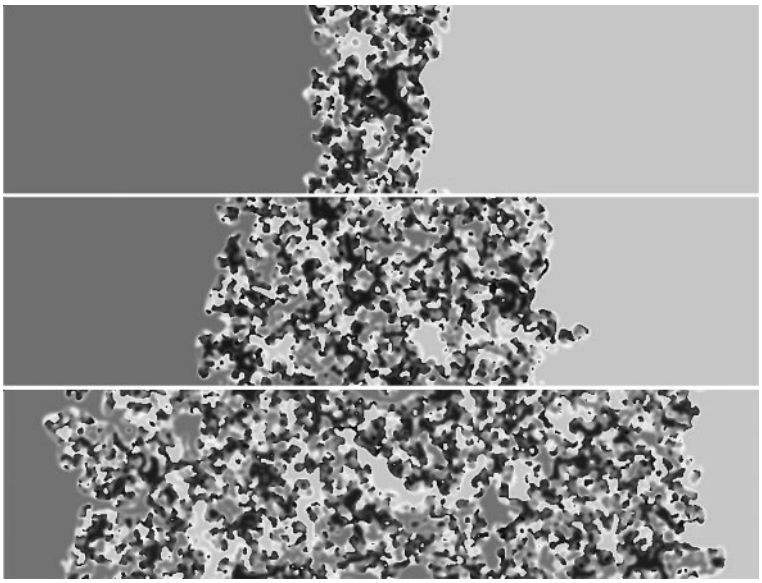

Fig. 11 The interface in a system with $\gamma = 0.45$, in the strong turbulence regime, at $t = 500$, 1500 and 3000. The initial condition was a planar interface with a thin randomly-seeded strip. The grey-scale indicates the phase field ϕ of the complex amplitude $A = Re^{i\phi}$ with the darkest shade corresponding to $\phi = -\pi$ and the lightest corresponding to $\phi = +\pi$. The system size is 800 × 200.

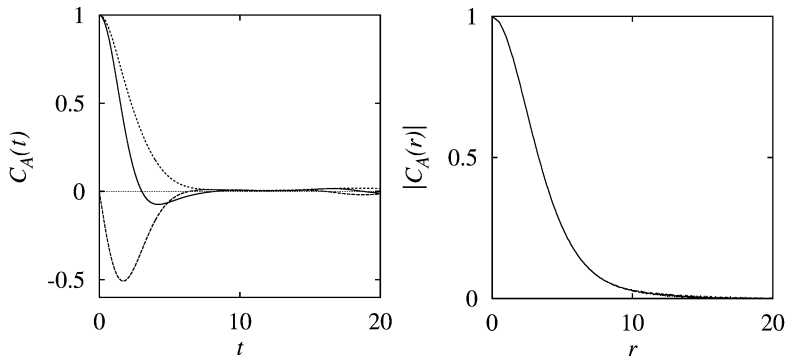

Fig. 12 Left: Temporal autocorrelation function. Real (solid line) and imaginary (dashed line) parts for $\gamma = 0.40$. The magnitude $|C_A(t)|$ is shown as a dotted line. Right: Spatial autocorrelation function for the same γ value. The imaginary part is close to zero and the real part is indistinguishable from $|C_A(r)|$ when plotted.

The results of this calculation are shown in Fig. 13. One can see that the width has a KPZ scaling structure.

5 Discussion and conclusions

We have found phase front dynamics in the 3 : 1 FCGL equation that are qualitatively similar to those reported in a coupled map lattice with period-3 local dynamics. In particular, we observed front roughening, thick fronts with complex internal structure and a "front-explosion", nonequilibrium phase transition.[16,18] In the CML these phenomena were associated with stable chaos. In contrast, we have shown that the FCGL equation exhibits deterministic chaos. When the internal turbulent structure is sufficiently developed, the fronts obey KPZ scaling. When the fronts are thin, however, the dynamics possess temporal and spatial correlations and the fronts no longer have KPZ scaling properties.

The CML dynamics of the thick fronts separating two homogeneous phases and the critical properties of the nonequilibrium phase transition were described well by a phenomenological stochastic model in which a turbulent phase was identified in the interfacial zone.[15] Consequently, the thick front may be decomposed into two interacting fronts (the left and right profiles of the thick front) separating the turbulent phase from the homogeneous phases. In this model Edwards–Wilkinson equations for the left and right profiles were coupled by terms describing the interaction between these profiles. Currently, investigations are in progress to characterize the critical properties of the FCGL phase transition. This should allow one to determine the validity of

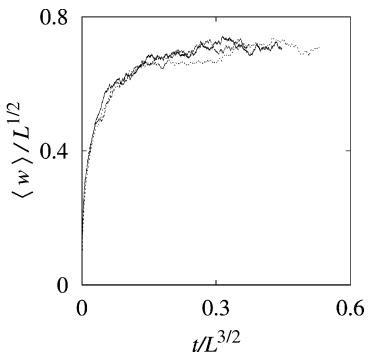

Fig. 13 Plot of $\langle w_h(t) \rangle / L^{1/2}$ *vs.* $t/L^{3/2}$ for system sizes $L = 500$ (solid curve), 400 (dashed curve) and 200 (dotted curve) for $\gamma = 0.43$. The $L = 400$ and $L = 500$ curves are averages over 100 realizations from initial conditions (9), the $L = 200$ curve is an average over 200 realizations.

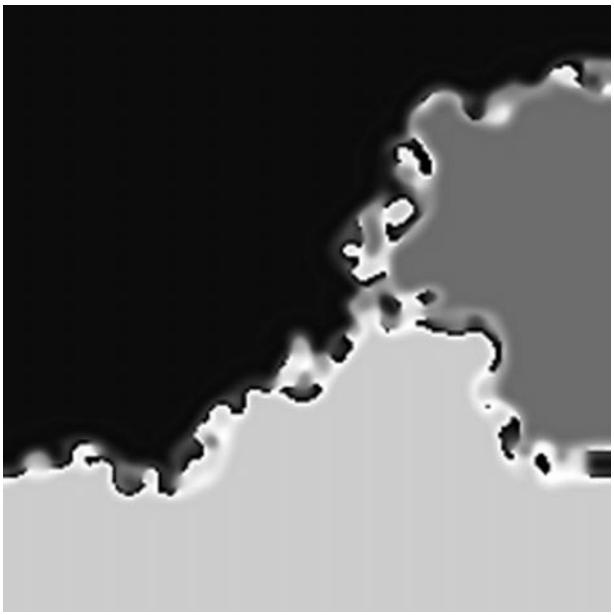

Fig. 14 The phase field ϕ in a simulation with $\gamma = 0.49$ from initial conditions containing a phase defect. The system size is 200×200.

phenomenological models of the form described above for the CML, and to shed light on the nature of the front explosion and its description as a nonequilibrium phase transition.

The phenomenology of the 3 : 1 FCGL equation in the Benjamin–Feir-unstable regime is remarkably rich. Some phenomena are similar to those previously found in the 2 : 1 FCGL equation while others have no known counterparts; however, there appears to be no reason why corresponding behaviour should not exist at other resonances.

The results presented here open a number of avenues for further investigation, both theoretical and experimental. Worthy candidates for investigation are the transition between what are apparently weakly turbulent and strongly turbulent regimes in the one-dimensional system, the zero-velocity holes and the origins of the non-KPZ scaling in the two-dimensional "thin front" regime. The nature of the bifurcation from constant-velocity motion to oscillatory motion in one-dimension is also an interesting question.

The FCGL equation is a sufficiently faithful model, as far as qualitative phenomenology is concerned, that there is a good likelihood that the phenomena described here also will exist in experimental 3 : 1 resonantly forced oscillatory systems. An experimental report of a 3-phase, phase-locked pattern in a light-sensitive Belousov–Zhabotinsky reaction shows 3 : 1 phase fronts that resemble the rough fronts in this study.[1]

Finally, we note that the foregoing study has been concerned entirely with phase fronts and has not considered other patterns that may exist in two-dimensional resonantly forced systems. Where three phases meet, one obtains three-armed spiral waves in which rough interfaces separate the arms (Fig. 14). Due to the constant nucleation and annihilation of phase defects in the turbulent interfaces, the situation is different from systems with regular dynamics where the single phase defect present may be identified with the spiral core. Instead, in systems with complex interfacial structure the core is a region with finite spatial extent. Since spiral dynamics plays an important role in reaction–diffusion systems, the investigation of the dynamics of these unusual spiral waves is a promising area for future research.

Acknowledgements

This work was supported in part by a grant from the Natural Sciences and Engineering Research Council of Canada.

References

1 V. Petrov, Q. Ouyang and H. L. Swinney, *Nature*, 1997, **388**, 655.
2 V. Petrov, M. Gustaffson and H. L. Swinney, in *Conference Proceedings of the 4th Experimental Chaos Conference*: August 6–8, 1997, Boca Raton, FL, USA, ed. M. Ding, W. Ditto, L. Pecora, S. Vohra and M. Spano, World Scientific, Singapore, 1998.
3 A. L. Lin, V. Petrov, H. L. Swinney, A. Ardelea and G. F. Carey, in *Pattern Formation in Continous and Coupled Systems*, The IMA Volumes in Mathematics and Its Applications, Vol. 115, ed. M. Golubitsky, D. Luss and S. H. Strogatz, Springer-Verlag, New York, 1999, p. 193.
4 A. L. Lin, A. Hagberg, A. Ardelea, M. Bertram, H. L. Swinney and E. Meron, *Phys. Rev. E*, 2000, **62**, 3790.
5 T. Kawagishi, T. Mizuguchi and M. Sano, *Phys. Rev. Lett*., 1995, **75**, 3768.
6 P. Coullet, J. Lega, B. Houchmanzadeh and J. Lajzerowicz, *Phys. Rev. Lett*., 1990, **65**, 1352.
7 J. M. Gambaudo, *J. Diff. Eqns*., 1985, **57**, 172.
8 C. Elphick, G. Iooss and E. Tirapegui, *Phys. Lett. A*, 1987, **120**, 459.
9 P. Coullet and K. Emilsson, in *Instabilities and Nonequilibrium Structures V*, ed. E. Tirapegui and W. Zeller, Kluwer, Dordrecht, 1996, p. 55.
10 P. Coullet and K. Emilsson, *Physica D*, 1992, **61**, 119.
11 P. Coullet and K. Emilsson, *Physica A*, 1992, **188**, 190.
12 For examples of studies of phase fronts in the Benjamin–Feir-stable regime see: (*a*) C. Elphick, A. Hagberg, B. A. Malomed and E. Meron, *Phys. Lett. A*, 1997, **230**, 33; (*b*) C. Elphick, A. Hagberg and E. Meron, *Phys. Rev. Lett*., 1998, **80**, 5007.
13 T. Mizuguchi and S. Sasa, *Prog. Theor. Phys*., 1993, **89**, 599.
14 D. Battogtokh and D. A. Browne, *Phys. Lett. A*, 2000, **266**, 359.
15 R. Kapral, R. Livi and A. Politi, *Phys. Rev. Lett*., 1997, **79**, 2277.
16 R. Kapral, R. Livi, G.-L. Oppo and A. Politi, *Phys. Rev. E*, 1994, **49**, 2009.
17 Y. Cuche, R. Livi and A. Politi, *Physica D*, 1997, **103**, 369.
18 A. Politi, R. Livi, G.-L. Oppo and R. Kapral, *Europhys. Lett*., 1993, **22**, 571.
19 J. H. Merkin, V. Petrov, S. K. Scott and K. Showalter, *Phys. Rev. Lett*., 1996, **76**, 546.
20 H. L. Barabási and H. E. Stanley, *Fractal Concepts in Surface Growth*, Press Syndicate of the University of Cambridge, New York, 1995.
21 S. F. Edwards and D. R. Wilkinson, *Proc. R. Soc. London, Ser. A*, 1982, **381**, 17.
22 M. Kardar, G. Parisi and Y.-C. Zhang, *Phys. Rev. Lett*., 1986, **56**, 889.
23 G. Benettin, L. Galgani and J.-M. Strelcyn, *Phys. Rev. A*, 1976, **14**, 2338.